Journal of Atmospheric and Solar-Terrestrial Physics 177 (2018) 274–282

Contents lists available at ScienceDirect

Journal of Atmospheric and Solar-Terrestrial Physics

journal homepage: www.elsevier.com/locate/jastp

# A case study comparing citizen science aurora data with global auroral boundaries derived from satellite imagery and empirical models

Burcu C. Kosar[a,b,*], Elizabeth A. MacDonald[a,b], Nathan A. Case[c], Yongliang Zhang[d], Elizabeth J. Mitchell[d], Rodney Viereck[e]

[a] New Mexico Consortium, Los Alamos, NM, USA
[b] NASA Goddard Space Flight Center, Greenbelt, MD, USA
[c] Department of Physics, Lancaster University, UK
[d] JHU Applied Physics Laboratory, Laurel, MD, USA
[e] NOAA Space Weather Prediction Center, Boulder, CO, USA

ARTICLE INFO

*Keywords:*
Auroral equatorward boundaries
Empirical models
Citizen science

ABSTRACT

Aurorasaurus is a citizen science project that offers a new, global data source consisting of ground-based reports of the aurora. For this case study, aurora data collected during the 17–18 March 2015 geomagnetic storm are examined to identify their conjunctions with Defense Meteorological Satellite Program (DMSP) satellite passes over the high latitude auroral regions. This unique set of aurora data can provide ground-truth validation of existing auroral precipitation models. Particularly, the solar wind driven, Oval Variation, Assessment, Tracking, Intensity, and Online Nowcasting (OVATION) Prime 2013 (OP-13) model and a Kp-dependent model of Zhang-Paxton (Z-P) are utilized for our boundary validation efforts. These two similar models are compared for the first time.

Global equatorward auroral boundaries are derived from the OP-13 model and the DMSP Special Sensor Ultraviolet Spectrographic Imager (SSUSI) far ultraviolet (FUV) data using the Z-P model at a fixed flux level of 0.2 erg $cm^{-2}$ $s^{-1}$. These boundaries are then compared with citizen science reports as well as with each other. Even though there are some large differences between the global boundaries for a few cases, the average difference is about 1.5° in geomagnetic latitude, with OP-13 being equatorward of Z-P model. When these boundaries are compared with each other as a function of local time, no clear overall trend as a function of local time was observed. It is also found that the ground-based reports are more consistent with the predictions of the OP-13 model.

## 1. Introduction

The coupling of solar wind plasma into the Earth's magnetosphere leads to the precipitation of particle flux into the high latitude regions of the Earth's ionosphere. The optical manifestation of this complex chain of physical processes is the aurora. Early morphological studies of the aurora established that various auroral forms (e.g., arcs, bands) are distributed into an oval configuration globally around the Earth's magnetic pole (Feldstein, 1964; Feldstein and Starkov, 1967; Feldstein and Starkov, 1968). The spatial and temporal variations of auroral oval boundaries provide information on the state of the near-Earth space environment. Early studies showed that the changing auroral oval is a manifestation of changing internal structure of the magnetosphere (Akasofu, 1966). Furthermore, Nakai and Kamide (1983) and Boudouridis et al. (2003) investigated the auroral oval dynamics in response to the interplanetary magnetic field (IMF) and the solar wind dynamic pressure, respectively. Nakai and Kamide (1983) found that the equatorward boundary during periods of southward IMF is generally at lower latitudes than during northward IMF. Using particle precipitation data from DMSP spacecraft, Boudouridis et al. (2003) found that solar wind dynamic pressure changes can dramatically affect the auroral oval location, size, and intensity. Therefore, an accurate description of the auroral oval boundaries is of great importance to our understanding of magnetospheric and ionospheric physics as well as space weather.

Auroral oval predictions are generally based on data collected by various space-based particle detectors or imagers and their incorporation into empirical models that make predictions of the precipitation patterns (Evans, 1987; Hardy et al., 1985, 1989; 1991; Zhang and Paxton, 2008; Newell et al., 2010a, 2014; Mitchell et al., 2013). In this

* Corresponding author. New Mexico Consortium, Los Alamos, NM, USA.
*E-mail address:* bkosar@my.fit.edu (B.C. Kosar).

https://doi.org/10.1016/j.jastp.2018.05.006
Received 27 May 2017; Received in revised form 18 May 2018; Accepted 21 May 2018
Available online 24 May 2018

study, the spatial and temporal behavior of energy flux are obtained from the OP-13 model (Newell et al., 2010a, 2014) and the DMSP/SSUSI FUV observations using the Z-P model (Paxton et al., 1992, 2002; Zhang and Paxton, 2008). This is the first study comparing the boundary predictions of these two similar empirical models. OP-13 is an auroral precipitation model (Newell et al., 2014) that uses a highly accurate solar wind-magnetosphere coupling function (Newell et al., 2007) to produce high resolution energy flux maps between 50° to 90° magnetic latitude in both hemispheres. It is the improved version of the original OVATION Prime 2010 (OP-10) model (Newell et al., 2010). The Z-P model is an empirical Kp-dependent model developed using 4 years of Global Ultraviolet Imager (GUVI) data and Epstein function fitting method formerly used by Hardy et al. (1987). A global auroral boundary is also derived from each model at a specific level of energy flux.

Aurorasaurus actively collects thousands of ground-based reports of the aurora globally and incorporates them into scientific investigations as a new data source (MacDonald et al., 2015). This unique data set offer ground-truth validation for the predictions of empirical models. A recent study by Case et al. (2016a) compared a subset of Aurorasaurus citizen science data with the operational forecast of the visible aurora provided by National Oceanic and Atmospheric Administration's (NOAA) Space Weather Prediction Center (SWPC). The aurora forecast product of SWPC utilizes the output from the OP-10 model for estimating the location of the most equatorial latitude of the visible aurora known as the view-line. This study demonstrated that 60% of the positive aurora reports collected by Aurorasaurus were equatorward of the view-line predicted by SWPC. This finding led to defining a new, less conservative Aurorasaurus view-line (Case et al., 2016a; b).

For the 17–18 March 2015 geomagnetic storm we have identified and examined approximately 120 citizen science reports that are in conjunction with DMSP F16, F17 and F18 satellite passes. Global auroral boundaries obtained from the OP-13 and the Z-P models are compared with citizen science reports as well as with each other. Unlike earlier work, here we focus on the boundaries at fixed flux levels overhead, not the view-line which corresponds to aurora that may be visible on the horizon.

It is important to note that FUV cameras on satellites and all-sky cameras on the ground do not measure the same physical signatures of aurora Sigernes et al. (2011). There are extensive networks of all-sky camera data on the ground, though they are limited by cloud coverage and land mass, as are Aurorasaurus data, generally. Currently auroral boundaries from these networked cameras are not regularly extracted. Such work is of future interest but generally beyond the scope of current data processing methods. The use of Aurorasaurus observers as “ground truth” is appropriate for the analysis methods chosen in this paper, which is in comparison to two models both based on space-borne measurements of auroral proxies for a large event. Large geomagnetic events are those which are the most rare, and therefore have the least frequent data (and thus highest uncertainties) going into building statistical auroral models. The Aurorasaurus data are most plentiful for large events, and we begin with a case study to best illustrate the utility and potential of this technique.

## 2. Citizen science aurora data during the 17–18 March 2015 geomagnetic storm

On 17 March 2015, a coronal mass ejection (CME) hit the Earth causing an intense geomagnetic storm. The signature of the geomagnetic storm was apparent as significant fluctuations in many interplanetary and geophysical parameters. In Fig. 1 variations of Dst, Kp, IMF Bz, and solar wind speed with the storm commencement and evolution are shown. During the main phase of the storm (section highlighted with gray), solar wind speed increases while the IMF Bz turns southward. The Dst index decreases and reaches a minimum of −223 nT around 22:00 UT on 17 March 2015, which marks the beginning of the recovery phase (section highlighted with yellow). The Kp index briefly reached 8 during the main phase of the storm. This particular period of strong geomagnetic activity was chosen for this case study because it offers dynamically varying auroral oval boundaries with the storm evolution and elevated number of reports (Case et al., 2015a; b). Fig. 2 shows that the number of citizen science aurora reports submitted to Aurorasaurus during the St. Patrick's day storm is significantly larger (about 12 times) than the daily average number of reports (~20 during quiet times). This figure also demonstrates that the number of observations peak particularly during enhanced geomagnetic storm conditions (Kp ≥ 4). A case study of such an active period with an abundance of reports (total of 241) increases the likelihood of finding conjunctions with the DMSP satellite passes. This is explained further in Section 4.

During the storm period, Aurorasaurus collected 241 reports via the project's website and apps. All reports include a timestamp, a location, and frequently they include meta-data describing the observed aurora (such as color, type etc.) as well as the local environmental conditions. Aurorasaurus data consists of direct reports submitted to the project via its website and apps and tweets that are mined from Twitter via keyword searching and place name geo-location or native geo-tagging. Direct reports submitted to the project can either be a positive or a negative sighting, depending on if the observer saw the aurora or not. These data are then scanned thoroughly for data integrity issues. For example, one common error is that users select an incorrect end time for their observations (e.g. 11am rather than 11pm). To mitigate this particular error, if the difference between the start and end time of the observation exceeds 3-hrs we filter out these reports due to not complying with the real-time data standard of the project. Another example is that a positive sighting is reported from a region where an aurora sighting is incredibly unlikely (e.g. southern US states during a minor storm). We assume that this is the result of an error in completing the location field and thus such reports are also filtered out. Negative sightings that are of interest to this case study must indicate clear, unobscured view of the sky. Furthermore, the duplicates of all direct reports are excluded.

Data from Twitter reports is extracted using a rigorous process as described by Case et al. (2016c). In summary, it is a two-step process: verification and validation. First, the aurora related and geo-tagged tweets are presented on the project website to our user community. They are asked to verify the real-time aspect of the tweet by up or down voting on them. Following the verification step, the validity of user-verified tweets are manually checked by the Aurorasaurus team members. Team members are trained to validate tweets using a standard protocol based on the same set of tweets that were used during the project's first validation effort as described in detail in Case et al. (2016c). During this manual validation, the positively verified tweets are analyzed one at a time. For each tweet, the team members inspect the tweet's text, any links associated with the tweet (which usually includes an image), and the location and time information of the tweet to determine any signs of non-original content. During this inspection, each tweet is cross-checked against other observations (e.g. reports submitted directly to Aurorasaurus and other known sightings) and the predictions of solar wind driven auroral models for the same time period for accurate classification. Inspected tweets are then sorted into two major categories: valid or invalid. The valid category represents tweets that are identified by Aurorasaurus users as real-time aurora sightings and are confirmed by the trained Aurorasaurus team members. The invalid category is a collection of tweets that, according to the Aurorasaurus team members, are misidentified as real-time aurora sightings by the user community. The Aurorasaurus project only uses the valid category of positive verified tweets in scientific analysis.

After this two-step process, a tweet is classified as a positively verified tweet. Quality control measures are an important part of citizen science project design. In multiple fields, data collected by “amateurs” has been shown to be as accurate as “traditional” sources (Sullivan

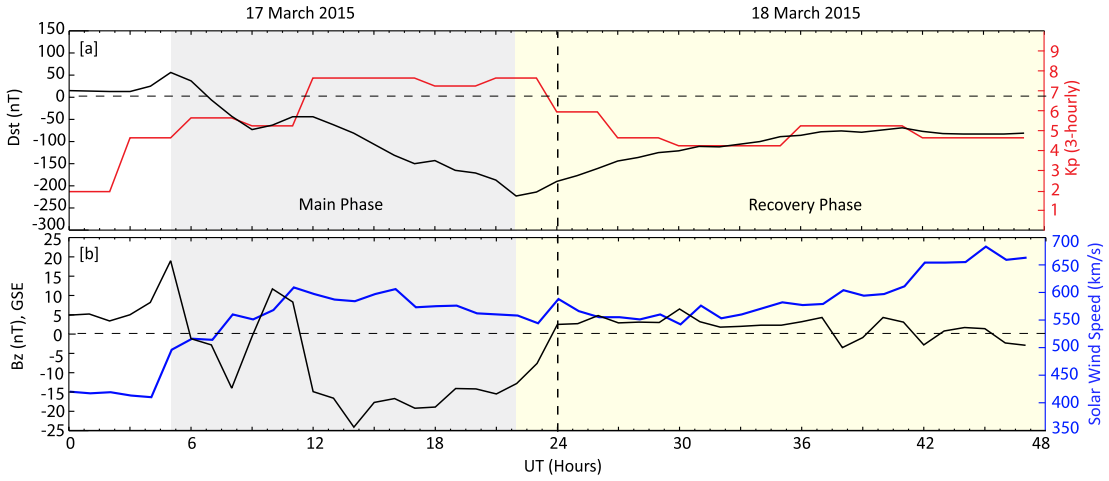


**Fig. 1.** Variation of (a) Dst (black curve) and Kp (red curve) indices and (b) IMF Bz (black curve) and solar wind speed (blue curve) during 17–18 March 2015. All data are obtained from the OMNI data set provided by NASA Goddard Space Flight Center. Except the Kp index (3-hourly average), all parameters are hourly averaged. The vertical dashed line separates the days. The gray and yellow shaded regions correspond to the main and the recovery phases of the storm, respectively. (For interpretation of the references to color in this figure legend, the reader is referred to the Web version of this article.)

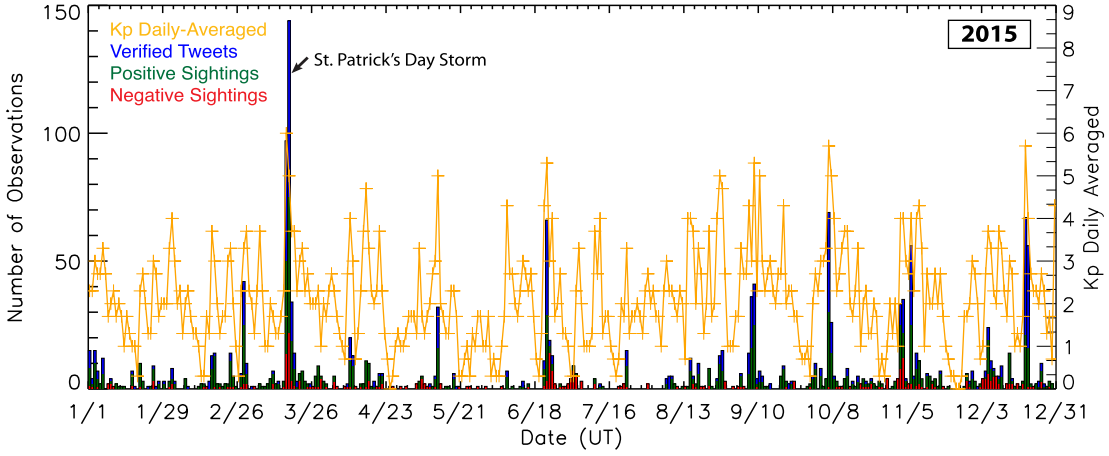


**Fig. 2.** A stack plot of the Aurorasaurus citizen science data collected during the year of 2015. The number of daily citizen science observations is plotted on the y-axis along with the maximum daily Kp value on the secondary y-axis.

et al., 2009; Meentemeyer et al., 2015). There are numerous measures in place for various aspects of the Aurorasaurus project for both quality control and assurance. For this paper, the dataset is checked for quality using the methods described earlier and the analysis is restricted to appropriate time windows for both citizen science and satellite data outlined in Section 4. This follows standards for data usage specifically the best practice of "fitness for use", ensuring that the uncertainty in time in both data sources are accounted for appropriately. Then, we draw results based primarily on analysis in aggregate with some representative cases providing additional context. The naturally fine scale aurora can vary significantly during the time of a polar satellite pass (~20 min). This is an important caveat to any conjunction analysis with asynchronous data sources.

## 3. Global auroral boundary derivation from empirical models and satellite imagery

Aurora is the end result of a complex coupling between the solar wind, magnetosphere, and ionosphere. There are, therefore, a number of physical parameters associated with the dynamics of it and, subsequently, with global auroral models. The relevant parameter for the current comparison study is the location of the equatorward auroral boundary. However, there are many different ways this boundary can be defined. Case et al. (2016a) defined this boundary as the latitude at which the percent probability of visible aurora in the SWPC OVATION product is greater than 18%. This value is equivalent to $\sim 1\ \mathrm{erg\ cm^{-2}\ s^{-1}}$ which is defined as a threshold value for the visible aurora by Machol et al. (2012). The definition criteria that we use for the equatorward boundary is also threshold-based but is adopted from Zhang and Paxton (2008) who define it at a fixed flux level of $0.2\ \mathrm{erg\ cm^{-2}\ s^{-1}}$. Sigernes et al. (2011) also used the same threshold value for the equatorward boundary and noted that increasing this threshold value would cut the low flux contributions both poleward and equatorward of the auroral oval. It is important that both models are evaluated at the same threshold value.

### 3.1. DMSP/SSUSI FUV observations and Zhang-Paxton model

For the 17–18 March 2015 geomagnetic storm, we have examined aurora data from three DMSP satellites: F16, F17, and F18. The DMSP satellites were launched in a polar, sun-synchronous orbit around the Earth at an altitude of 850 km. The SSUSI instrument periodically images a portion of the auroral oval every 98 min over both Northern and Southern hemispheres. The scan mirror sweeps the 16 spatial pixel footprint from horizon to horizon perpendicular to the spacecraft motion, producing one frame of 16 cross-track lines in 22 s (Paxton et al.,

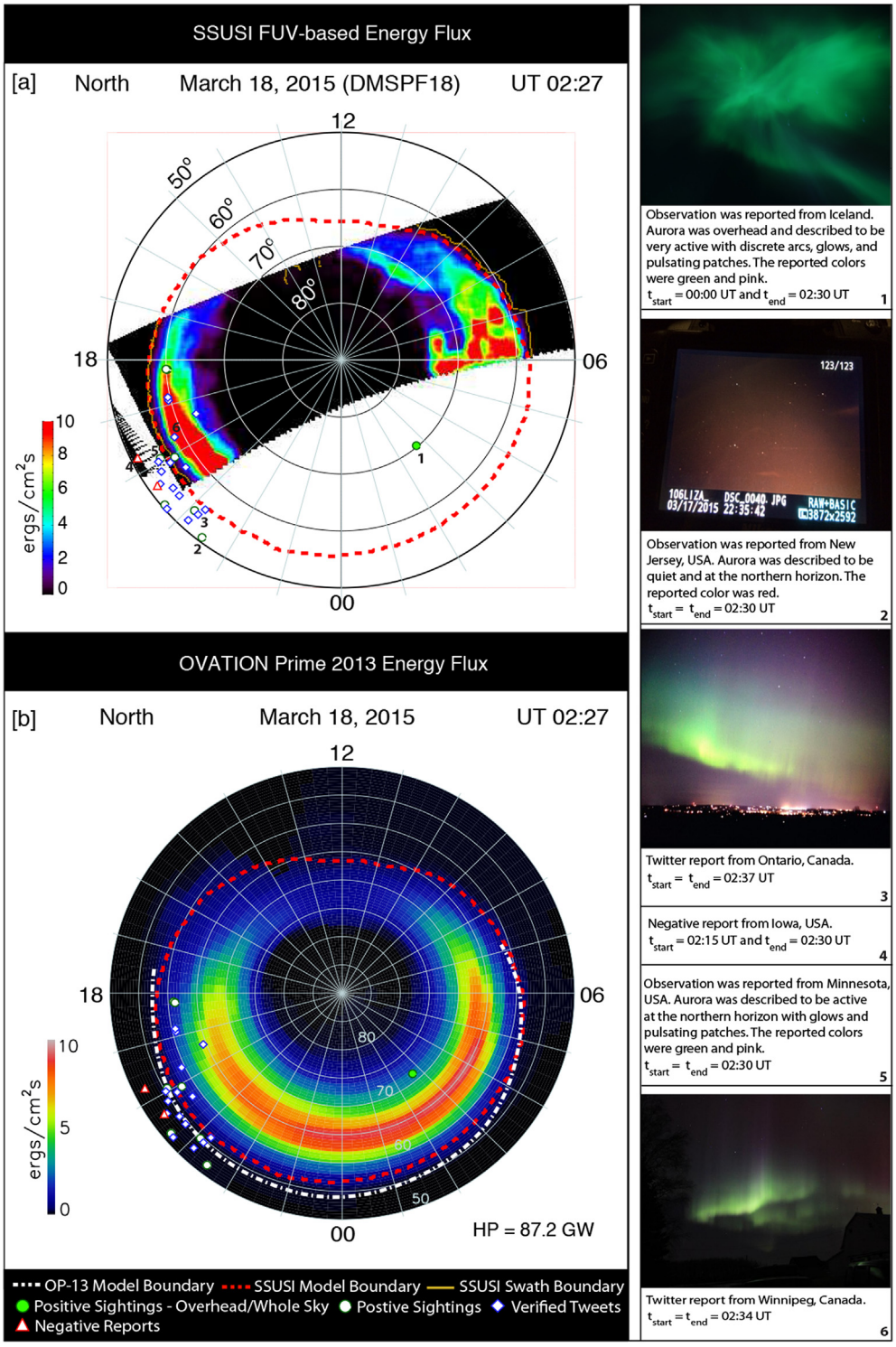


**Fig. 3.** Plot of citizen science data together with [a] the auroral energy flux map obtained from FUV image captured by the SSUSI instrument on board DMSP-F18 satellite and [b] the output of the summed energy flux ($\sum j$) for four auroral types predicted by the OP-13 auroral precipitation model for 18 March 2015 at 02:27 UT. The yellow solid line outlining the FUV image is the SSUSI swath boundary. 26 citizen science reports that fall within the conjunction criteria include all types of reports. For illustrating report contents, we have numbered a few from one to six in Panel [a]. A detailed description of each report is given in the boxes with corresponding numbers on the right (additional metadata and precise location are typically available). (For interpretation of the references to color in this figure legend, the reader is referred to the Web version of this article.)

1992). The SSUSI imager completes its scanning of the pole in about ~20 min. A timestamp is given to each pass identifying the time of the highest magnetic latitude pixel ($t_{pole}$) in the FUV image. During the 48 h of interest, we identified 94% of the data collected by the three satellites to be suitable for further analysis. We note that some of the SSUSI files are partial for some orbits due to downlink issues.

The SSUSI instrument is able to image the auroral precipitation patterns at different wavelengths in FUV including $N_2$ Lyman-Birge-Hopfield Short (LBHS, 140–150 nm) and $N_2$ Lyman-Birge-Hopfield Long (LBHL, 165–180 nm) that are produced by the precipitating electrons

upon their impact with the upper atmosphere (Zhang and Paxton, 2008; Zhang et al., 2010). Following the example of Strickland et al. (1983), the intensities of LBHS and LBHL are converted to maps of mean energy ($E$) and flux ($Q$) of precipitating electrons by utilizing the output from various ionospheric transport codes. Once the energy flux maps are produced, the equatorward boundary of the aurora at 0.2 erg $cm^{-2}$ $s^{-1}$ is outlined by a yellow solid line (see Fig. 3) and referred to as the SSUSI swath boundary.

The Kp-dependent, FUV-based empirical auroral model of Zhang and Paxton (2008) was developed using the data collected between the years of 2002–2005 by the GUVI instrument which is operationally very similar to the SSUSI instrument. The four years of GUVI data is also processed similarly to SSUSI and thousands of $E$ and $Q$ maps were produced. These maps are then binned into six pre-selected ranges of Kp (0–1.5, 1.5–3.0, 3.0–4.5, 4.5–6.0, 6.0–8.0 and 8.0–10.0) representing various geomagnetic disturbance levels. The mean energy and flux of precipitating electrons with changing Kp is found by fitting Epstein functions (Hardy et al., 1987) to the binned data (Zhang and Paxton, 2008). The global model boundary is obtained by selecting the Z-P model boundary that has the best match with the SSUSI swath boundary on the nightside (at magnetic local times from 18:00 to 06:00).

### 3.2. OVATION prime 2013 (OP-13) model

OP-13 is a statistical auroral precipitation model that was developed using in-situ measurements of positive and negative particles (32 eV–30 keV) by DMSP SSJ/4 or SSJ/5 detectors. The particle data are separated into 4 auroral types (monoenergetic, broadband, diffuse electron, and ion) and a linear regression fit is done between the energy flux and the Newell et al. (2007) solar wind-magnetosphere coupling function. This coupling function is an estimate of dayside merging rate and given by

$$d\Phi_{MP}/dt = v^{4/3}B_T^{2/3}\sin^{8/3}(\theta/2) \quad (1)$$

where $v$ is the solar wind speed, $B_T = \sqrt{B_y^2 + B_z^2}$ is the component of magnetic field transverse to Earth-Sun line, and $\theta = \arctan(B_y/B_z)$ is the IMF clock angle. The OP-13 model grid is 0.25-hrs magnetic local time (MLT) (96 bins) by 0.5° magnetic latitude (MLAT) (80 bins x 2 hemispheres) between 50° and 90° MLAT. The post-midnight region (00:15 to 03:30 MLT and 55° to 69° MLAT) has insufficient data to be modeled due to the sun-synchronous orbits of the DMSP satellite constellation. To compensate, the OP-13 model linearly interpolates across this gap using available data and neighboring bins (Newell et al., 2014).

The OP-10 model is limited due to the relative paucity of data from very active times. The most notable difference in the OP-13 model is the improvement of the limitations of OP-10 under strong geomagnetic conditions using GUVI total energy fluxes in conjunction with the previously derived ratios of auroral types for a given grid cell. If the solar wind-magnetosphere coupling function, $d\Phi_{MP}/dt$, exceeds the value of $1.2 \times 10^6$ Wb/s (corresponding to 61 GW or roughly $Kp$= 5 + or 6-), OP-13 runs in this “high activity mode” (Newell et al., 2014).

To be able to obtain the equatorward fixed flux level boundary, we run the OP-13 model for each of the SSUSI/DMSP satellite passes at the $t_{pole}$ times. For each MLT bin, we determined the minimum magnetic latitude at which the value of precipitating energy flux drops to the value of 0.2 erg $cm^{-2}$ $s^{-1}$. The set of coordinates representing the fixed flux level boundary are then smoothed and clipped at the day/night terminators.

## 4. Comparison results

To accurately compare the citizen science reports with simultaneous DMSP passes over the Northern hemisphere, it was necessary to determine conjunction criteria. We select citizen science auroral observations that occurred within ± 10 min of the $t_{pole}$ time of each pass. Since the $t_{pole}$ time occurs around 90° MLAT, ± 10 min would represent the time it takes for the SSUSI instrument to complete its total scan of the auroral oval and hence is a suitable time window for extracting conjugate aurora reports. Observations are extracted if their start time ($t_{start}$) or end time ($t_{end}$) fall within the conjunction criteria. This conjunction criteria reduces the SSUSI data and Aurorasaurus reports down to 36 out of 78 passes (46%) and 112 out of 241 reports (46%), respectively. We note that there is significant paucity with both data sources, namely Aurorasaurus data are sparse and do not cover all local times equally. Secondly, DMSP satellites provide less than complete coverage of the auroral oval.

Fig. 3 shows an example conjunction. Citizen science data is plotted with the auroral energy flux map obtained from the inversion of FUV images captured by the SSUSI instrument on 18 March 2015 at $t_{pole}$ of 02:27 UT (in Fig. 3[a]). The corresponding output of the summed energy flux predicted by the OP-13 for the same time is plotted in Fig. 3[b]. Both figures are plotted in geomagnetic coordinates and on the similar color scales. The hemispheric power of 87.2 GW predicted by OP-13 suggests a strong disturbance level.

This particular case was identified as an ideal case for detailed discussion for three reasons: (1) relatively good coverage of the auroral oval by the SSUSI instrument in the pre-midnight sector (between 18:00–21:00 MLT), (2) the highest number of citizen science reports available (total of 26) that satisfy the conjunction criteria, and (3) approximately 40% of the reports fall within the FUV image of the auroral oval captured by the SSUSI imager. This example includes all possible report types each denoted with a filled circle (i.e. 2 negative report, 9 positive sightings, and 15 verified tweets are shown with red, green, and blue, respectively). Six citizen science reports are labeled and their detailed descriptions are given in boxes with corresponding numbers on the right side of Fig. 3. There were 9 positive sighting in total. One of them around ~70° MLAT described the aurora as overhead and eight of them described it to be either at 45° North or close to the Northern horizon. The observed aurora was mostly green with diffuse glows and pulsating patches and 25% of the reports included an image.

The SSUSI swath boundary (yellow solid line) along with the fixed flux level boundaries obtained from the Z-P (red dashed line) and the OP-13 (white dashed line) models are also shown in Fig. 3[a] and 3[b]. The Z-P and OP-13 boundaries agree well in local times 2-hrs after dusk and 2-hrs before dawn, however, the agreement is slightly poorer outside of this range and the separation between the two boundaries increases towards midnight. Looking at citizen science data, ~35% of the reports fall inside, ~30%. fall in the close vicinity, and ~35% fall outside of the model boundaries predicted by the Z-P and OP-13 models. The auroral reports are expected to be significantly equatorward of an overhead boundary due to the height of the aurora in the sky, so this is not inconsistent necessarily. These trends for multiple passes are examined in more detail next.

### 4.1. Comparison between OP-13 and SSUSI model boundaries

In aggregate, the fixed flux level boundaries obtained from the Z-P and OP-13 models for the 36 conjunctions are compared with each other and the magnetic latitude difference between the two is plotted as a function of magnetic local time in Fig. 4[a]. The 36 conjunctions are split into two categories depending on the value of the Newell's solar wind coupling function ($d\Phi_{MP}/dt$) being above or below $1.2\times10^6$ Wb/s (~. 61 GW) corresponding to the threshold for OP-13's high activity mode. If the Z-P boundary is at a higher latitude than the OP-13, this leads to a positive difference while the reverse scenario leads to a negative difference. Overall, there is no clear trend as a function of local time for either category, therefore it is unlikely that the largest differences are due to irregularities in OP-13 high or low activity mode.

The magnetic latitude difference between the two boundaries is

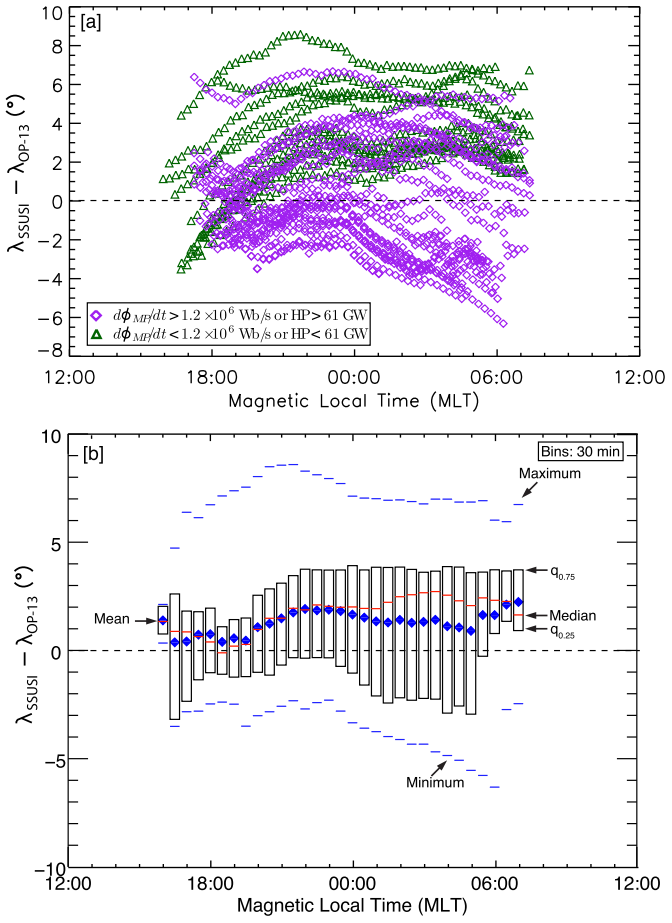


**Fig. 4.** [a] The magnetic latitude differences between the fixed flux level boundaries obtained from the Z-P and OP-13 models for the 36 conjunctions are shown as a function of magnetic local time. [b] The magnetic latitude differences between the two boundaries are binned into 30 min magnetic local time bins and average within each bin is found. Various other parameters representing the distribution of data in each magnetic local time bin are also shown.

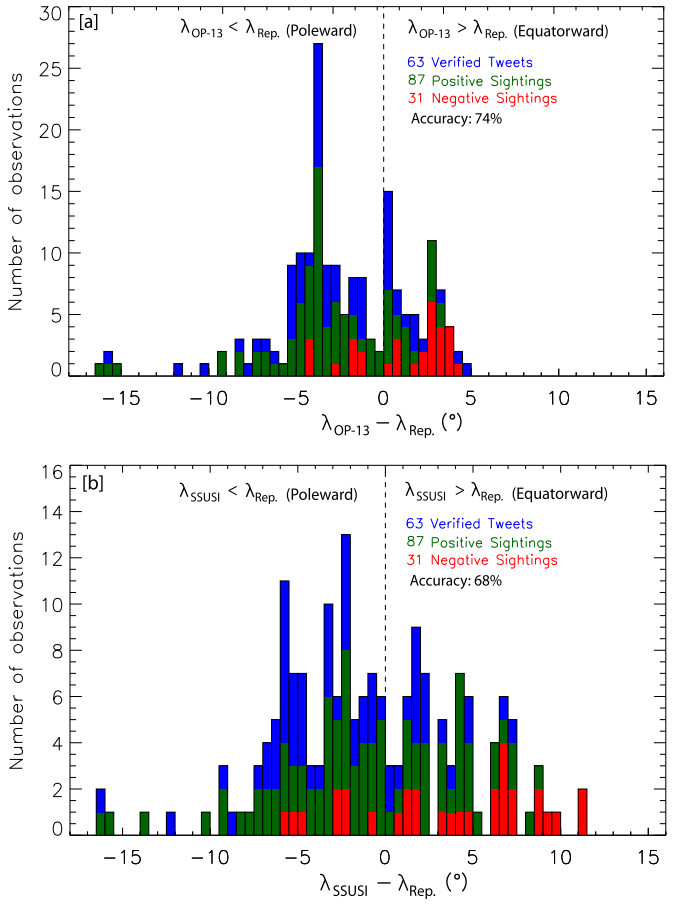


**Fig. 5.** Histogram plots showing the distribution of latitude difference between citizen science reports ($\lambda_{Rep.}$) with fixed flux level boundaries obtained from [a] OVATION Prime 2013 model ($\lambda_{OP-13}$) and [b] Zhang-Paxton empirical auroral model ($\lambda_{SSUSI}$). The stacked bars represent number of different types of reports (red: negative reports, green: positive sightings, and blue: verified tweets) in each 0.5° geomagnetic latitude bins. (For interpretation of the references to color in this figure legend, the reader is referred to the Web version of this article.)

then binned into 0.5-hrs MLT bins and the average within each bin is found. Even though there are some large differences between the fixed flux level boundaries for a few cases, on average the SSUSI boundary is about 1.5° poleward compared to the OP-13 boundary (in Fig. 4[b]).

### 4.2. Comparison of citizen science reports with model boundaries

Next, we compare the reports to the boundaries for all 36 conjugate passes during 17–18 March 2015, which span the main and recovery phases of the geomagnetic storm. Fig. 5 shows the distribution of latitude difference between the citizen science reports and the conjugate fixed flux level boundaries obtained from the two different empirical models discussed earlier. If the report is equatorward of the boundary, it leads to a positive latitude difference; if the report is poleward of the boundary then the latitude difference is negative.

The quality assessment for each boundary can be performed by calculating the accuracies of each relative to citizen science reports using a statistical technique suggested by Machol et al. (2012) as ACC = $(\sum TP + \sum TN)/\sum N$ where $\sum TP$ are the total number of true positive reports that fall within, $\sum$ TN are the total number of true negative reports that fall outside of the fixed flux level boundary, $\sum$ N are the total number of reports. This equation yields an accuracy (ACC) of approximately 74% for the OP-13 and 68% for the Z-P boundaries.

The earlier study by Case et al. (2016a) for this period found the accuracy of the equatorial boundary of the OP-13 model to be 49.7%. The lower relative accuracy is reasonable considering that their equatorial boundary was defined as the latitude at a higher flux level of 1 erg $cm^{-2}$ $s^{-1}$. Observers can often see aurora far equatorward due to its height in the sky and that they might observe sub-visual aurora due to their camera's exposure time and sensitivity. In both studies with citizen science reports, no attempt has been made to quantitatively define a sensitivity threshold of seeing aurora. However, in aggregate, models can be compared to these reports meaningfully to examine their consistency with quantitative boundaries.

## 5. Discussion

Fig. 4[b] shows that the Z-P boundary is on average a few degrees more poleward than the OP-13 boundary. Fig. 5 shows that the ground-based reports appear slightly more consistent with the OP-13 boundary. This is the first attempt to quantitatively compare these boundaries to each other and to observer data. Future study can examine a broader range of this data. A few more representative cases are examined to provide context of the relative comparison.

### 5.1. Conjunction cases

The auroral oval varies dynamically during a geomagnetic storm and validation of the models and their boundaries is quite challenging.

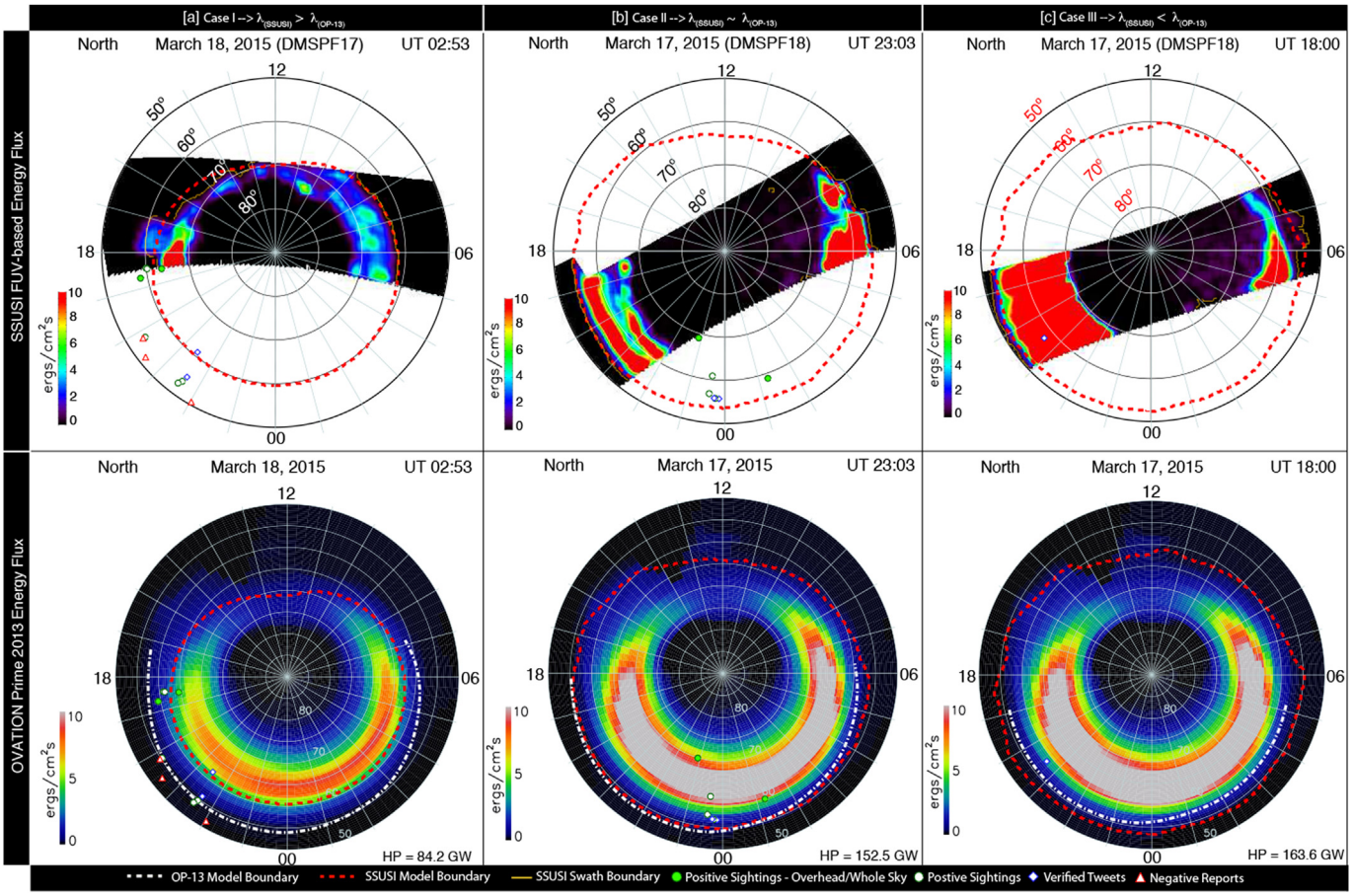


**Fig. 6.** Three typical cases [a] $\lambda_{SSUSI} > \lambda_{OP-13}$, [b] $\lambda_{SSUSI} \sim \lambda_{OP-13}$, and [c] $\lambda_{SSUSI} < \lambda_{OP-13}$ are identified from 36 conjunctions to emphasize the differences and similarities between data and models. Top panel shows the auroral energy flux map obtained from FUV images captured by the SSUSI instrument on board DMSP satellites F-17 and F-18 during 17–18 March 2015 for three different conjunctions. Bottom panel shows the output of the summed energy flux ($\sum j$) for four auroral types predicted by OP-13 auroral precipitation model for the same conjunction times. The Zhang-Paxton model boundary is shown on both panels for ease of comparison.

In this section, a few other cases demonstrate some of these validation challenges by comparing the Z-P model boundary with the predictions of the OP-13 auroral precipitation model as well as the aurora data collected by Aurorasaurus for the same conjunction time.

Space-based FUV imagers, such as SSUSI, can diagnose the instantaneous state of the auroral oval. However, SSUSI images are composed of partial segments of the oval along the track of a low-altitude polar orbiting satellite. Images of partial oval segments lead to certain caveats while deriving the auroral boundaries from them. Obtaining reliable model boundaries from the SSUSI data depend on two factors: (1) the size of the segment that falls within the nightside and (2) the clarity and sharpness of the FUV images. To be able to demonstrate the effects of these factors, three typical cases are identified from the 36 conjunctions.

Fig. 6[a] shows the first case (18 March 2015 - UT 02:53) analyzed. Most of the satellite track falls on the dayside with a relatively smaller region on the nightside. Overall, the imaged aurora shows a discontinuous spatial pattern. The swath boundary location obtained from such a non-uniform oval configuration affects the derivation of the Z-P model boundary. For the same conjunction time, the summed energy flux of precipitating electrons predicted by the OP-13 model leads to a more equatorward boundary at the same flux level. The modeled peak energy flux intensity of the OP-13 model is lower on the dusk side (~18:00 MLT) and higher on the dawn side (~06:00 MLT) compared to the SSUSI flux.

The auroral data collected by citizen scientists are also displayed on the same map and can serve as ground-truth helping to validate the boundaries predicted by the models. In Fig. 6[a] most of the reports seem to agree better with the boundary prediction of the OP-13 as opposed to the Z-P model boundary. The reports are distributed consistently in a sense that the negative reports fall outside of both boundaries, while the positive reports are distributed in close vicinity or at a higher magnetic latitude compared to the fixed flux level boundary of the OP-13 model. One of the positive reports indicating an overhead aurora is coincident with the section of the auroral oval around ~64° MLAT. The other overhead observation around ~58° MLAT is outside of the oval imaged by the SSUSI or predicted by the OP-13. This case is representative of a category where the SSUSI model boundary is at a significantly higher latitude than OP-13 (i.e. $\lambda_{SSUSI} > \lambda_{OP-13}$). This could be due to the variation of auroral forms with local time. In this particular case, the imaged oval contributing to the global boundary derivation is mostly on the dawn sector where aurora tends to be more discontinuous with patchy or diffuse aurora. This likely leads to a less accurate extrapolation to the location of the global Z-P boundary.

We have identified another case (17 March 2015 - UT 23:03) that is shown in Fig. 6[b]. For this particular case, the dusk half of the satellite track fully samples a large section of the auroral oval and the entire swath is on the nightside. The dawn half of the track also has a good coverage but it is mostly the dayside aurora hence not contributing to the Z-P model boundary derivation. The large nightside swath leads to a Z-P model boundary that is mostly close to the OP-13 (i.e. $\lambda_{SSUSI} \sim \lambda_{OP-13}$) boundary. However, there are some differences to point out compared to Case I: in Case-II the fully sampled section of the auroral oval (1) is mostly continuous with sharp equatorial edges that

leads to a uniform, consistent swath boundary and (2) the section of the oval sampled on the nightside is significantly larger (covers between 18:30–21:30 MLT). Therefore, the size of the sampled auroral oval on the night side as well as its spatial continuity seem to be important factors affecting the swath boundary and in turn the model boundary. For this conjunction time, all citizen science observations fall poleward of both boundaries. There is one positive report with the mention of aurora being overhead or whole sky from ~70° MLAT that is within the predicted OP-13 oval but outside of the imaged oval. Note that the SSUSI FUV images represent a snapshot of the auroral oval, however, aurora can vary very quickly. The possible reason for this offset between the citizen science report and the poleward swath boundary is that the auroral oval could have expanded significantly right after the passage of the satellite in a very short time.

Compared to Case II, the auroral oval imaged on 17 March 2015 - UT 18:00 (see Fig. 6[c]) is almost twice as wide (~ 18° in MLAT). Similar to Case II, it is continuous with a large nightside swath. The Z-P model boundary is consistently few degrees equatorward of the OP-13 boundary across all local times (i.e. $\lambda_{SSUSI} < \lambda_{OP-13}$).

The three cases analyzed suggest that aurora is subject to large local variations that can not be fully captured by satellite imagers or predicted by empirical models. Empirical models primarily utilize highly averaged auroral data or maps that cover wide ranges of geomagnetic conditions to perform their statistical calculations. Newell's solar wind coupling function ($d\Phi_{MP}/dt$) is calculated using the solar wind conditions averaged from the last 4 h that is strongly weighed towards the last hour. The Z-P model boundary derivation is affected by the quality and the nightside coverage of the SSUSI FUV images. In addition, there are model related issues that also affect the accuracy of the derived boundary discussed in Zhang and Paxton (2008).

## 6. Conclusions

For one of largest geomagnetic storms of solar cycle 24, 36 conjunction examples are identified and examined. The number of conjunctions is constrained by both available citizen science reports and the DMSP satellite pass times. During the two day initial period of this storm, 241 reports were collected by Aurorasaurus, however, only 46% of these reports are conjunctive with this case study. While the availability of citizen science ground-truth data are still sparse, the utility of these techniques is demonstrated. With its globally distributed, fast growing citizen science community, Aurorasaurus is a new, potential demonstration for this boundary validation analysis. The frequency of citizen science report submission correlates with geomagnetic activity and the number of project followers. In certain regions, existing local communities with a high number of observers show great potential for the continuity of crowd-sourced reports.

Even though there are some large differences between the global boundaries for a few cases, the average difference is about 1.5° in geomagnetic latitude, with OP-13 being equatorward of Z-P model. When these boundaries are compared with each other as a function of local time, no clear overall trend was observed. Comparison of the citizen science reports with fixed flux level boundaries obtained from Z-P and OP-13 empirical auroral models yielded accuracies of 68% and 74%, respectively. Using citizen science data as a ground-truth, the OP-13 boundary is slightly more consistent for the cases and parameters examined.

The SSUSI FUV images appear to be limited by orbital coverage in magnetic local time. Most of the cases produce good SSUSI model fits, however, poor fits are potentially due to the coverage area not coinciding with the nightside. Future work aims to utilize a broader dataset to assess a quality flag for the SSUSI boundary fit. Low Earth Orbiting (LEO) satellite coverage is inherently limited compared to other orbits (e.g. IMAGE, POLAR etc.). Equally, ground reports are also inherently limited due to the observers' distribution, local conditions, e.g. cloud coverage. Citizen science data for the year of 2015 and 2016 is available to provide ground truth.

It is important to note that there are significant differences between these data sources in terms of auroral morphology. OP-13 represents a statistical average of the auroral region and as such does not take into account the dynamic contribution from substorms. SSUSI FUV images of the aurora are limited by magnetic local time coverage, but inherently show higher resolution auroral structure. Compared to both OP-13 and SSUSI, Aurorasaurus data collected from citizen scientists in real-time represent the finest scale but are also limited in space and time coverage. Currently, most of the Aurorasaurus reports are from the populated areas of the high latitude regions of the northern hemisphere therefore extending this study to validate auroral boundaries in the southern hemisphere is challenging. However, the project has outreach efforts to expand its user-base to the southern hemisphere to provide better global coverage for the ground-truth data in the near future. Having enough observations to statistically compare for a small event is a challenge. Therefore, currently there is no ideal platform that can capture the high resolution dynamics of the aurora and this limits space weather knowledge. A promising option is to combine data from various different sources and models to develop a new, hybrid assimilative platform. An assimilative approach may significantly improve our real-time knowledge of the system scale state of the aurora.

## Acknowledgments

This material is based upon work supported, in part, by the National Science Foundation under grant 1344296. Any opinions, findings, and conclusions or recommendations expressed in this material are those of the author(s) and do not necessarily reflect the views of NSF. Nathan A. Case is supported by STFC grant number ST/M001059/1. The Aurorasaurus citizen science data used in this study can be obtained by contacting the corresponding author. The OVATION Prime output was kindly provided by the Space Weather Prediction Center (Boulder, CO) of the National Oceanic and Atmospheric Administration (NOAA), U.S. Department of Commerce. The output can be freely downloaded from the NOAA SWPC product pages (http://www.swpc.noaa.gov/products/aurora-30-minute-forecast). The SSUSI data products were kindly provided by the Johns Hopkins University Applied Physics Laboratory and can be downloaded from the SSUSI instrument pages (http://ssusi.jhuapl.edu). The OMNI data were obtasined from the GSFC/SPDF OMNIWeb interface at http://omni web.gsfc.nasa.gov. The Aurorasaurus citizen science data used in this study can be obtained by contacting the corresponding author.

## Appendix A. Supplementary data

Supplementary data related to this article can be found at http://dx.doi.org/10.1016/j.jastp.2018.05.006.

## References

Akasofu, S.I., 1966. The auroral oval, the auroral substorm, and their relations with the internal structure of the magnetosphere. Planet. Space Sci. 14, 587–595.
Boudouridis, A., Zesta, E., Lyons, R., Anderson, P., Lummerzheim, D., 2003. Effect of solar wind pressure pulses on the size and strength of the auroral oval. J. Geophys. Res.: Space Physics 108.
Case, N., MacDonald, E., Heavner, M., Tapia, A., Lalone, N., 2015a. Mapping auroral activity with Twitter. Geophys. Res. Lett. 42, 3668–3676.
Case, N.A., Kingman, D., MacDonald, E.A., 2016b. A real-time hybrid aurora alert system: combining citizen science reports with an auroral oval model. Earth and Space Science 3, 257–265.
Case, N.A., MacDonald, E.A., McCloat, S., Lalone, N., Tapia, A., 2016c. Determining the accuracy of crowdsourced tweet verification for auroral research. Citiz. Sci. Theory Pract. 2016.
Case, N.A., MacDonald, E.A., Patel, K.G., 2015b. Aurorasaurus and the St. Patrick's day storm. Astron. Geophys. 56, 3–13.
Case, N.A., MacDonald, E.A., Viereck, R., 2016a. Using citizen science reports to define the equatorial extent of auroral visibility. Space Weather.
Evans, D., 1987. Global Statistical Patterns of Auroral Phenomena. pp. 325–330.
Feldstein, Y., Starkov, G., 1967. Dynamics of auroral belt and polar geomagnetic

disturbances. Planet. Space Sci. 15, 209–229.
Feldstein, Y.I., 1964. Auroral morphology, I. The location of the auroral zone. Tellus 16, 252–257.
Feldstein, Y.I., Starkov, G., 1968. Auroral oval in the IGY and IQSY period and a ring current in the magnetosphere. Planet. Space Sci. 16, 129–133.
Hardy, D.A., Gussenhoven, M., Brautigam, D., 1989. A statistical model of auroral ion precipitation. J. Geophys. Res.: Space Physics 94, 370–392.
Hardy, D.A., Gussenhoven, M., Holeman, E., 1985. A statistical model of auroral electron precipitation. J. Geophys. Res.: Space Physics 90, 4229–4248.
Hardy, D.A., Gussenhoven, M., Raistrick, R., McNeil, W., 1987. Statistical and functional representations of the pattern of auroral energy flux, number flux, and conductivity. J. Geophys. Res.: Space Physics 92, 12275–12294.
Hardy, D.A., McNeil, W., Gussenhoven, M., Brautigam, D., 1991. A statistical model of auroral ion precipitation: 2. Functional representation of the average patterns. J. Geophys. Res.: Space Physics 96, 5539–5547.
MacDonald, E.A., Case, N.A., Clayton, J.H., Hall, M.K., Heavner, M., Lalone, N., Patel, K.G., Tapia, A., 2015. Aurorasaurus: a citizen science platform for viewing and reporting the aurora. Space Weather 13, 548–559.
Machol, J.L., Green, J.C., Redmon, R.J., Viereck, R.A., Newell, P.T., 2012. Evaluation of OVATION Prime as a forecast model for visible aurorae. Space Weather 10.
Meentemeyer, R.K., Dorning, M.A., Vogler, J.B., Schmidt, D., Garbelotto, M., 2015. Citizen science helps predict risk of emerging infectious disease. Front. Ecol. Environ. 13, 189–194.
Mitchell, E., Newell, P., Gjerloev, J., Liou, K., 2013. OVATION-SM: a model of auroral precipitation based on superMAG generalized auroral electrojet and substorm onset times. J. Geophys. Res.: Space Physics 118, 3747–3759.
Nakai, H., Kamide, Y., 1983. Response of nightside auroral-oval boundaries to the interplanetary magnetic field. J. Geophys. Res.: Space Physics 88, 4005–4014.
Newell, P., Liou, K., Zhang, Y., Sotirelis, T., Paxton, L., Mitchell, E., 2014. OVATION Prime-2013: extension of auroral precipitation model to higher disturbance levels. Space Weather 12, 368–379.
Newell, P., Sotirelis, T., Liou, K., Meng, C.I., Rich, F., 2007. A nearly universal solar wind-magnetosphere coupling function inferred from 10 magnetospheric state variables. J. Geophys. Res.: Space Physics 112.
Newell, P.T., Sotirelis, T., Wing, S., 2010. Seasonal variations in diffuse, monoenergetic, and broadband aurora. J. Geophys. Res.: Space Physics 115.
Paxton, L.J., Meng, C.I., Fountain, G.H., Ogorzalek, B.S., Darlington, E.H., Gary, S.A., Goldsten, J.O., Kusnierkiewicz, D.Y., Lee, S.C., Linstrom, L.A., et al., 1992. Special sensor ultraviolet spectrographic imager: an instrument description. In: San Diego'92, International Society for Optics and Photonics, pp. 2–15.
Paxton, L.J., Morrison, D., Zhang, Y., Kil, H., Wolven, B., Ogorzalek, B.S., Humm, D.C., Meng, C.I., 2002. Validation of remote sensing products produced by the Special Sensor Ultraviolet Scanning Imager (SSUSI): a far UV-imaging spectrograph on DMSP F-16. In: International Symposium on Optical Science and Technology, International Society for Optics and Photonics, pp. 338–348.
Sigernes, F., Dyrland, M., Brekke, P., Chernouss, S., Lorentzen, D.A., Oksavik, K., Deehr, C.S., 2011. Two methods to forecast auroral displays. Journal of Space Weather and Space Climate 1 A03.
Strickland, D., Jasperse, J., Whalen, J., 1983. Dependence of auroral FUV emissions on the incident electron spectrum and neutral atmosphere. J. Geophys. Res.: Space Physics 88, 8051–8062.
Sullivan, B.L., Wood, C.L., Iliff, M.J., Bonney, R.E., Fink, D., Kelling, S., 2009. ebird: a citizen-based bird observation network in the biological sciences. Biol. Conserv. 142, 2282–2292.
Zhang, Y., Paxton, L., 2008. An empirical Kp-dependent global auroral model based on TIMED/GUVI FUV data. J. Atmos. Sol. Terr. Phys. 70, 1231–1242.
Zhang, Y., Paxton, L.J., Bilitza, D., Doe, R., 2010. Near real-time assimilation in IRI of auroral peak E-region density and equatorward boundary. Adv. Space Res. 46, 1055–1063.